

# Linear Attention for Joint Power Optimization and User-Centric Clustering in Cell-Free Networks

Irched Chafaa, Giacomo Bacci, Senior Member, IEEE, Luca Sanguinetti, Fellow, IEEE

**Abstract**—Optimal access point (AP) clustering and power allocation are critical in user-centric cell-free massive MIMO systems. Existing deep learning models lack flexibility to handle dynamic network configurations. Furthermore, many approaches overlook pilot contamination and suffer from high computational complexity. In this paper, we propose a lightweight transformer model that overcomes these limitations by jointly predicting AP clusters and powers solely from spatial coordinates of user devices and APs. Our model is architecture-agnostic to users load, handles both clustering and power allocation without channel estimation overhead, and eliminates pilot contamination by assigning users to APs within a pilot reuse constraint. We also incorporate a customized linear attention mechanism to capture user-AP interactions efficiently and enable linear scalability with respect to the number of users. Numerical results confirm the model’s effectiveness in maximizing the minimum spectral efficiency and providing near-optimal performance while ensuring adaptability and scalability in dynamic scenarios.

**Index Terms**—CosFormer, Transformer, linear attention, supervised learning, power optimization, user-centric cell-free massive MIMO.

## I. Introduction

Cell-free massive MIMO (mMIMO) has emerged as a promising architecture to overcome the limitations of conventional cellular networks [1]–[4]. Unlike traditional cellular systems, where each user equipment (UE) is associated with a single base station, cell-free mMIMO deploys a large number of distributed access points (APs) that coherently and jointly serve all UEs within the coverage area. This high level of cooperation offers uniform service quality, mitigates inter-cell interference, and enhances spectral efficiency (SE), particularly in dense or heterogeneous environments. However, realizing these benefits in practice remains challenging. If every AP serves every UE, the resulting system demands substantial fronthaul signaling, creates unnecessary interference from weak AP-UE links, and leads to inefficient use of power and pilot resources [5].

The authors are with the Dipartimento di Ingegneria dell’Informazione, University of Pisa, Via Caruso 16, 56122, Pisa, Italy (e-mail: irched.chafaa@ing.unipi.it, {giacomo.bacci, luca.sanguinetti}@unipi.it). This work was supported by the Smart Networks and Services Joint Undertaking (SNS JU) under the European Union’s Horizon Europe research and innovation program under Grant Agreement No 101192369 (6G-MIRAI), and by the project FoReLab (Departments of Excellence), funded by the Italian Ministry of Education and Research (MUR).

To address these challenges, the user-centric paradigm has been introduced in cell-free mMIMO [6]–[9]. In this approach, each UE is served by a subset of the most relevant APs, selected based on spatial proximity or channel quality. By restricting cooperation to the most beneficial APs, the user-centric strategy reduces interference and enhances scalability by lowering the computational and signaling burden. Nevertheless, the performance of user-centric cell-free mMIMO depends critically on the proper selection of AP clusters and transmission powers, which must adapt dynamically to variations in channel conditions, UE mobility, and network configurations. This makes clustering and power control crucial challenges in realizing the full potential of user-centric cell-free mMIMO.

## A. Related work

Given the importance of clustering and power optimization in user-centric cell-free mMIMO, a wide range of solutions have been proposed in the literature [6], [10]–[18]. These approaches differ in whether they treat clustering and power allocation separately or jointly, and in the methodologies employed, ranging from classical optimization to modern machine learning.

Classical optimization-based methods have long been applied to power allocation, often through iterative algorithms [6], [10] or closed-form solutions for specific objectives such as the max-min fairness (MMF) problem [11]. While these approaches can achieve near-optimal performance, they typically require multiple iterations to converge, resulting in high computational complexity and poor scalability in dynamic networks.

In parallel, clustering strategies have been studied extensively. Heuristic approaches [12], [13] provide simple rules for grouping users and APs, while optimization-based formulations [14] aim for more principled solutions. More recently, deep learning models [15] have been introduced to automate clustering decisions. Despite their advantages, these methods often lack adaptability: heuristic rules may oversimplify, optimization approaches remain computationally demanding, and deep learning solutions require retraining whenever the number of UEs or APs changes.

Joint clustering and power allocation has also been investigated [16]–[18], with the goal of simultaneously determining the serving AP subset and transmission powers. These methods generally outperform separate treatments, but they still suffer from scalability issues and often neglect critical aspects such as pilot contamination.

Overall, whether treated separately or jointly, existing solutions remain limited in their ability to adapt efficiently to dynamic network conditions.

### B. Transformer-based power allocation

Recently, Transformers [19] have been explored to address flexibility in dynamic wireless networks. In [20], the authors propose a transformer-based model for only down-link (DL) power allocation to handle varying numbers of UEs via unsupervised learning. However, the proposed method requires post-processing and padding, which introduces excessive padding when user loads vary widely, potentially diluting meaningful information, and increases computational load without contributing useful information [21], [22], thereby slowing training and affecting convergence. In [23], we addressed the flexibility issue in cell-free mMIMO by leveraging a transformer-based model capable of handling varying network configurations without padding or retraining. Unlike [20], which employs large-scale fading coefficients as input, our model uses only spatial information (AP/UE coordinates) to jointly predict up-link (UL) and DL powers. This design enables efficient adaptation to changes in the number of UEs and APs, while maintaining near-optimal performance for the MMF problem. Nevertheless, the solution did not address AP clustering or pilot contamination, and its complexity still scaled quadratically with the number of users similarly to [20]. In summary, the key question motivating this work is: How can we overcome these limitations while preserving the advantages of Transformer-based models in dynamic cell-free mMIMO?

### C. Main contributions

Building on our earlier work in [23], this paper addresses the limitations previously identified. We introduce a deep learning model, termed exponential linear unit (ELU)-CosFormer, which takes UE and AP coordinates as input and jointly predicts AP clusters and UL/DL power levels. The model employs a customized linear attention mechanism tailored to the spatial and structural characteristics of the prediction task, ensuring scalability and robustness in dynamic network conditions. The learning framework is trained in a supervised manner to maximize the minimum SE, thereby promoting UE fairness while inherently eliminating pilot contamination without requiring additional processing.

The main contributions of this work can be summarized as follows:

- Joint clustering and UL/DL power control: The proposed model learns to jointly predict the AP clusters serving each UE together with the corresponding UL/DL power levels. This joint design suppresses interference from irrelevant AP-UE links and improves the utilization of limited resources such as power, signaling, and computation. By relying solely on spatial information, the model minimizes overhead

and decouples clustering and power control from data detection, while remaining robust to variations in network load.

- Customized linear attention via ELU-CosFormer: We modify the attention mechanism of CosFormer [24], a Transformer variant with linear attention complexity, and benchmark it against other linear Transformer architectures [24]–[27]. In the proposed variant, the rectified linear unit (ReLU) activation in the attention kernel is replaced with ELU, providing smoother gradients, enhanced numerical stability, and improved convergence under noisy or heterogeneous input conditions.
- Pilot contamination elimination: The attention mechanism is embedded within a constrained encoder, which enforces that each AP serves no more UEs than the number of available orthogonal pilots. By integrating this constraint directly into the architecture, the model inherently avoids pilot contamination and mitigates interference, without relying on additional pilot-assignment procedures or coordination overhead.
- Robustness to input uncertainty: We also examine a key deployment aspect that has been overlooked in prior Transformer-based approaches [20], [23]: robustness to input uncertainty. In practical systems, AP/UE coordinates are subject to estimation errors; to model this, we perturb the input positions with Gaussian noise of varying intensity. The results demonstrate that the proposed model maintains stable and reliable performance across a broad range of noise levels, highlighting its robustness to imperfect spatial information and its suitability for real-world deployment.

### D. Reproducible research

The code used for model design and training will be provided upon request and will be made publicly available after the review process is complete.

### E. Paper outline and notation

The remainder of the paper is organized as follows. Sects. II and III describe the wireless network model and the problem formulation. Sect. IV introduces the proposed ELU-CosFormer architecture for AP clustering and power optimization, while Sect. V details the training procedure. Sect. VI presents an extensive performance evaluation, and Sect. VII provides a computational complexity analysis. Conclusions and potential future extensions are discussed in Sect. VIII.

We denote the sets of real and complex numbers by  $\mathbb{R}$  and  $\mathbb{C}$ . Matrices and vectors are written in boldface upper- and lowercase letters, respectively. The superscript  $(\cdot)^H$  denotes the Hermitian operator, and  $\odot$  indicates element-wise multiplication. Element indices are written as  $a_i$  for the  $i$ th entry of vector  $\mathbf{a}$  and  $a_{i,j}$  for the  $(i,j)$ th entry

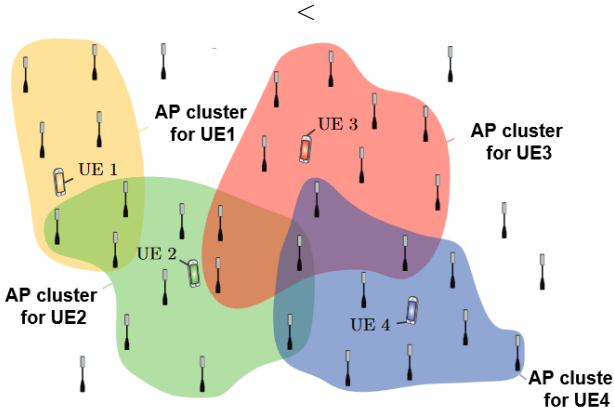


Fig. 1: Illustration of a user-centric cell-free mMIMO network. Each UE is served by its own cluster of APs [6].

of a matrix. The notation  $\mathcal{N}_C(\mathbf{m}, \mathbf{C})$  refers to a circularly symmetric complex Gaussian variable with mean  $\mathbf{m}$  and covariance matrix  $\mathbf{C}$ . The norm  $\|\cdot\|$  denotes the  $\ell_2$  vector norm, and  $\mathbb{E}[\cdot]$  the expectation operator. The notation  $\mathbb{1}(\cdot)$  refers to the indicator function.

## II. Wireless Network Model

We consider a user-centric cell-free mMIMO network, shown in Fig. 1, with  $K$  single-antenna UEs and  $L$  APs, each having  $N$  antennas. Each UE is served by a subset of APs, and each AP can serve at most  $\tau_p$  UEs to prevent pilot contamination. The network operates under a standard time division duplexing (TDD) protocol [6], where the  $\tau_c$  symbols of each coherence block are allocated to UL training ( $\tau_p$ ), UL data ( $\tau_u$ ), and DL data ( $\tau_d$ ), with  $\tau_c \geq \tau_p + \tau_u + \tau_d$ . We adopt a narrowband channel model and assume that channels remain constant over a coherence block. The channel vector between AP  $l$  and UE  $k$  is denoted by  $\mathbf{h}_{lk}$  and modeled as [6]:

$$\mathbf{h}_{lk} = \sqrt{\beta_{lk}} \mathbf{R}_{lk}^{1/2} \mathbf{g}_{lk}, \quad (1)$$

where  $\beta_{lk}$  is the large-scale fading, accounting for path loss and shadowing,  $\mathbf{R}_{lk} \in \mathbb{C}^{N \times N}$  is the spatial correlation matrix at AP  $l$ , and  $\mathbf{g}_{lk} \sim \mathcal{N}_C(\mathbf{0}, \mathbf{I}_N)$  is an i.i.d. complex Gaussian vector representing the small-scale fading, where  $\mathbf{I}_N$  is the  $N \times N$  identity matrix. We assume that the channels  $\{\mathbf{h}_{lk}; l = 1, \dots, L\}$  are independent and call  $\mathbf{h}_k = [\mathbf{h}_{1k}^\top, \dots, \mathbf{h}_{Lk}^\top]^\top \in \mathbb{C}^{LN}$  the collective channel from all APs to UE  $k$ .

The central processing unit (CPU) computes the estimate of  $\mathbf{h}_k$  on the basis of received pilot sequences transmitted during the training phase [6]. The minimum mean square error (MMSE) estimate is  $\hat{\mathbf{h}}_k = [\hat{\mathbf{h}}_{1k}^\top, \dots, \hat{\mathbf{h}}_{Lk}^\top]^\top$  with [6, Sect. IV]

$$\hat{\mathbf{h}}_{lk} = \mathbf{R}_{lk} \mathbf{Q}_{lk}^{-1} \left( \mathbf{h}_{lk} + \frac{1}{\tau_p \rho} \mathbf{n}_{lk} \right) \sim \mathcal{N}_C(\mathbf{0}_N, \Phi_{lk}), \quad (2)$$

where  $\rho$  is the UL pilot power of each UE,  $\mathbf{n}_{lk} \sim \mathcal{N}_C(\mathbf{0}_N, \sigma^2 \mathbf{I}_N)$  is the thermal noise, and  $\Phi_{lk} = \mathbf{R}_{lk} \mathbf{Q}_{lk}^{-1} \mathbf{R}_{lk}$ , where  $\mathbf{Q}_{lk} = \mathbf{R}_{lk} + \frac{\sigma^2}{\tau_p \rho} \mathbf{I}_N$ . Hence,  $\hat{\mathbf{h}}_k \sim \mathcal{N}_C(\mathbf{0}_{LN}, \Phi_k)$ , with  $\Phi_k = \text{diag}(\Phi_{1k}, \dots, \Phi_{Lk})$ . Note that the method proposed in this paper can be applied to other channel estimation schemes.

### A. Uplink and downlink spectral efficiency

An achievable UL SE of UE  $k$  is given by the use-and-then-forget bound [6, Sect. V]:

$$\text{SE}_k^{\text{UL}} = \frac{\tau_u}{\tau_c} \log_2 \left( 1 + \text{SINR}_k^{\text{UL}} \right), \quad (3)$$

with the effective signal-to-interference-plus-noise ratio (SINR) defined as

$$\frac{p_k^{\text{UL}} |\mathbb{E}\{\mathbf{v}_k^\text{H} \mathbf{D}_k \mathbf{h}_k\}|^2}{\sum_{i=1}^K p_i^{\text{UL}} \mathbb{E}\{|\mathbf{v}_k^\text{H} \mathbf{D}_k \mathbf{h}_i|^2\} - p_k^{\text{UL}} |\mathbb{E}\{\mathbf{v}_k^\text{H} \mathbf{D}_k \mathbf{h}_k\}|^2 + \sigma^2 \mathbb{E}\{\|\mathbf{D}_k \mathbf{v}_k\|^2\}}. \quad (4)$$

Here,  $p_k^{\text{UL}}$  is the UL transmit power of user  $k$ ,  $\mathbf{v}_k \in \mathbb{C}^N$  is the combining vector, and  $\mathbf{D}_k = \text{diag}(\mathbf{D}_{k1}, \dots, \mathbf{D}_{kL})$  is a block-diagonal matrix with  $\mathbf{D}_{kl} = \mathbf{I}_N$  if AP  $l$  serves UE  $k$ , and zero otherwise. The expectation is taken with respect to all sources of randomness. Although the bound in (3) is valid for any combiner  $\mathbf{v}_k$ , we consider the MMSE, given by [6, Sect. V]:

$$\mathbf{v}_k = \left( \sum_{k=1}^K p_k^{\text{UL}} \hat{\mathbf{h}}_k \hat{\mathbf{h}}_k^\text{H} + \mathbf{Z} \right)^{-1} \hat{\mathbf{h}}_k, \quad (5)$$

where

$$\mathbf{Z} = \sum_{k=1}^K p_k^{\text{UL}} [\text{diag}(\mathbf{R}_{1k}, \dots, \mathbf{R}_{Lk}) - \Phi_k] + \sigma^2 \mathbf{I}_{LN}. \quad (6)$$

Similarly, the DL SE of user  $k$  is [6, Sect. VI]

$$\text{SE}_k^{\text{DL}} = \frac{\tau_d}{\tau_c} \log_2 \left( 1 + \text{SINR}_k^{\text{DL}} \right), \quad (7)$$

with effective SINR

$$\frac{p_k^{\text{DL}} |\mathbb{E}\{\mathbf{h}_k^\text{H} \mathbf{D}_k \mathbf{w}_k\}|^2}{\sum_{i=1}^K p_i^{\text{DL}} \mathbb{E}\{|\mathbf{h}_k^\text{H} \mathbf{D}_i \mathbf{w}_i|^2\} - p_k^{\text{DL}} |\mathbb{E}\{\mathbf{h}_k^\text{H} \mathbf{D}_k \mathbf{w}_k\}|^2 + \sigma^2}. \quad (8)$$

Here,  $p_k^{\text{DL}}$  is the DL power used by the CPU to serve UE  $k$  such that  $p_k^{\text{DL}} = \sum_{l=1}^L p_{k,l}^{\text{DL}}$ , with  $p_{k,l}^{\text{DL}} \in [0, \bar{P}_l^{\text{DL}}]$  being the AP  $l$ 's transmit power allocated for user  $k$ ;  $\bar{P}_l^{\text{DL}}$  is the maximum power per AP (when user  $k$  is not served by AP  $l$ ,  $p_{k,l}^{\text{DL}} = 0$ ); and  $\mathbf{w}_k \in \mathbb{C}^{LN}$  is the associated unit-norm precoding vector. The MMSE precoder is used [6], which is given by  $\mathbf{w}_k = \mathbf{v}_k / \|\mathbf{v}_k\|$ .

### III. Problem Formulation

To ensure fairness among UEs, we adopt the max-min fairness (MMF) problem, widely used in user-centric cell-free mMIMO systems [6], [11], [28]. In the UL, the problem takes the form [6, Sect. VII]:

$$\begin{aligned} & \max_{\{p_k^{\text{UL}} \geq 0\}} \min_k \text{SE}_k^{\text{UL}} \\ & \text{subject to } p_k^{\text{UL}} \leq \bar{P}_k^{\text{UL}} \quad \forall k \end{aligned} \quad (9)$$

where  $\bar{P}_k^{\text{UL}}$  is the maximum UL power for UE  $k$ . Similarly, in the DL we have that [6, Sect. VII]:

$$\begin{aligned} & \max_{\{p_k^{\text{DL}} \geq 0\}} \min_k \text{SE}_k^{\text{DL}} \\ & \text{subject to } \sum_{k=1}^K p_k^{\text{DL}} \leq \sum_{l=1}^L \bar{P}_l^{\text{DL}} \end{aligned} \quad (10)$$

where the constraint ensures that the total DL power allocated by the CPU does not exceed the overall network budget.

Although the optimization problems in (9) and (10) can be solved using closed-form solutions [11], iterative solvers [6], [10], or conventional deep learning models [20], [29], [30], existing methods suffer from two key limitations:

- 1) computational complexity that grows at least quadratically with  $K$ ;
- 2) lack of flexibility with respect to dynamic network loads.

These two drawbacks become critical in large-scale and time-varying networks. Hence, we propose a lightweight linear Transformer model, based on the CosFormer [24], that exploits only the spatial positions of UEs and APs to adaptively predict both serving clusters and powers while ensuring fairness and scalability under varying UE loads.

#### A. Overview of CosFormer

The standard Transformer [19] relies on an attention mechanism that captures dependencies among tokens (UEs in our case), but its quadratic complexity limits scalability. CosFormer [24] overcomes this issue by introducing a linearized attention mechanism that preserves accuracy while significantly reducing computational cost. Among linear Transformer variants [25]–[27], CosFormer is particularly well suited to our setting due to the following properties:

- 1) Accurate and stable attention: While many linear variants approximate the softmax attention and thus incur approximation errors, CosFormer replaces softmax with a cosine-based reweighting, improving numerical stability and avoiding such errors.
- 2) Implicit spatial bias: The cosine reweighting naturally emphasizes local relationships, which aligns with the importance of nearby AP-UE pairs for clustering and power allocation.

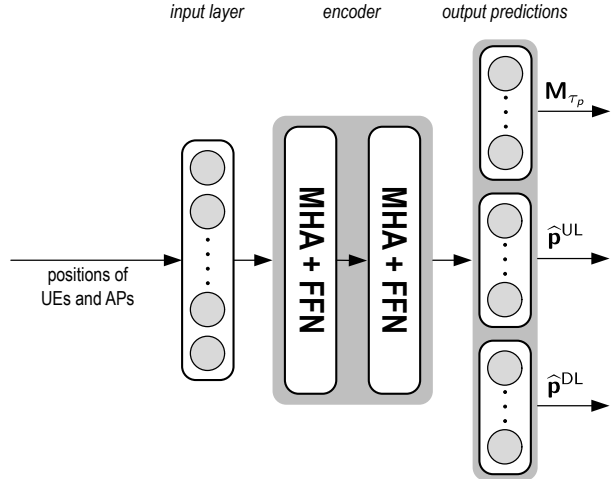


Fig. 2: Architecture diagram of the proposed model to predict jointly AP clusters, UL and DL powers leveraging spatial information at the input.

- 3) Computational efficiency: Through asymmetric projections, CosFormer attains linear complexity, reducing memory use and accelerating training, an essential feature for scalability in large cell-free networks.

Building on this foundation, we introduce our modified architecture, ELU-CosFormer, which augments CosFormer [24] with pilot-aware constraints and refined activation functions. These enhancements enable the model to jointly predict AP clusters and powers while eliminating pilot contamination and ensuring SE fairness. Once trained, ELU-CosFormer produces clusters and UL/DL power levels directly from the spatial positions of the UEs and APs, allowing seamless adaptation to varying network configurations without the need for retraining.

#### IV. Proposed Learning Model for Clustering and Power Optimization

In this section, we introduce the proposed learning model, ELU-CosFormer, which performs joint AP clustering and UL/DL power allocation. We first describe the overall model architecture and subsequently detail the linearized attention mechanism based on the modified CosFormer formulation.

##### A. Model architecture

The proposed model is a CosFormer-based neural network composed of three main components: a dynamic input layer, a stack of encoder layers, and parallel output heads for clustering and power prediction (see Fig. 2). These three components are described next in detail.

- 1) Input layer: The input tensor is  $\mathbf{X} \in \mathbb{R}^{K \times (2L+2)}$ , where each UE is represented by  $2L + 2$  spatial features (coordinates of all  $L$  APs and the UE itself).

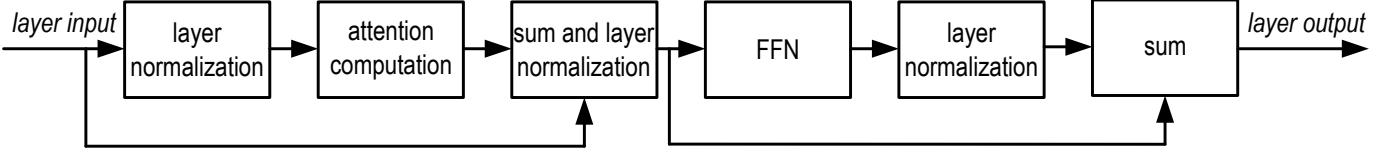


Fig. 3: Illustration diagram of operations in one encoder layer.

This tensor is projected into an embedding space of dimension  $d_{\text{mod}}$  via a linear layer:

$$\mathbf{Z}_{\text{in}} = \mathbf{X}\mathbf{W}_{\text{in}}^{\top} + \mathbf{b}_{\text{in}}, \quad (11)$$

with trainable parameters  $\mathbf{W}_{\text{in}}$  and  $\mathbf{b}_{\text{in}}$ . Through this dynamic embedding, the model handles seamlessly varying network sizes without architectural changes.

2) Encoder layers: The embedded tensor  $\mathbf{Z}^{(0)} = \mathbf{Z}_{\text{in}} \in \mathbb{R}^{K \times d_{\text{mod}}}$  is processed through  $M$  encoder layers. Each layer consists of a modified CosFormer multi-head attention (MHA), denoted by  $\mathcal{A}(\cdot)$ , followed by a feed-forward network (FFN). Moreover, the encoder layers apply layer normalization and residual connections to stabilize training and preserve information across layers [24]. Specifically, the  $m$ -th encoder layer applies the following operations (see Fig. 3):

$$\mathbf{Z}_1^{(m)} = \mathbf{Z}^{(m-1)} + \mathcal{A}(\tilde{\mathbf{Z}}^{(m-1)}), \quad (12)$$

$$\mathbf{H}^{(m)} = \text{ReLU}(\tilde{\mathbf{Z}}_1^{(m)} \mathbf{W}_1^{(m)\top} + \mathbf{b}_1^{(m)}), \quad (13)$$

$$\mathbf{Z}^{(m)} = \mathbf{Z}_1^{(m)} + \mathbf{H}^{(m)} \mathbf{W}_2^{(m)\top} + \mathbf{b}_2^{(m)}, \quad (14)$$

where  $\tilde{\mathbf{Z}}$  denotes a layer-normalized version of a tensor  $\mathbf{Z}$ ;  $\mathbf{W}_1^{(m)}$ ,  $\mathbf{b}_1^{(m)}$ ,  $\mathbf{W}_2^{(m)}$ , and  $\mathbf{b}_2^{(m)}$  are trainable parameters; ReLU refers to an activation function [31] introducing a non-linearity.

All  $M$  layers share the same structure and the output of each encoder layer preserves the dimension  $\mathbb{R}^{K \times d_{\text{mod}}}$ , serving as input to the next layer. After  $M$  layers, the final tensor  $\mathbf{Z}^{(M)} = \mathbf{Z}_{\text{out}}$  represents the encoder output that will be processed next by the output heads. The attention mechanism in (12) is detailed in Sect. IV-B.

3) Output heads: Three parallel heads operate on the final encoder output  $\mathbf{Z}_{\text{out}} \in \mathbb{R}^{K \times d_{\text{mod}}}$ :

- User-centric clustering mask: A fully-connected layer with sigmoid activation [31] produces an initial mask tensor  $\mathbf{M} \in \mathbb{R}^{K \times L}$ , where each entry represents the association strength between a UE and an AP:

$$\mathbf{M} = \text{sigmoid}(\mathbf{Z}_{\text{out}} \mathbf{W}_{\text{mask}} + \mathbf{b}_{\text{mask}}), \quad (15)$$

with trainable parameters  $\mathbf{W}_{\text{mask}}$  and  $\mathbf{b}_{\text{mask}}$ .

To mitigate pilot contamination, a two-step procedure is applied. First, for each AP, only the top  $\tau_p$  UEs with the highest mask scores are retained via  $\text{Top}_{\tau_p}(\mathbf{M})$ . Then, a thresholding operation assigns the AP to serve the UE if the retained score exceeds

a threshold  $\xi$ , yielding the final binary clustering mask:

$$\mathbf{M}_{\tau_p} = \mathbb{1}(\text{Top}_{\tau_p}(\mathbf{M}) \odot \mathbf{M} > \xi). \quad (16)$$

The threshold  $\xi$  is a hyperparameter tuned during training to balance connectivity and interference. Proper selection of  $\xi$  ensures strong UE-AP associations while maintaining high SE.

- Uplink power prediction: A fully-connected layer with sigmoid activation predicts normalized UL powers:

$$\tilde{p}_k^{\text{UL}} = \text{sigmoid}(\mathbf{Z}_{\text{out}} \mathbf{W}_{\text{UL}} + \mathbf{b}_{\text{UL}}), \quad (17)$$

- Downlink power prediction: Another fully-connected layer with sigmoid activation predicts normalized DL powers:

$$\tilde{p}_k^{\text{DL}} = \text{sigmoid}(\mathbf{Z}_{\text{out}} \mathbf{W}_{\text{DL}} + \mathbf{b}_{\text{DL}}), \quad (18)$$

where  $\mathbf{W}_{\text{UL}}$ ,  $\mathbf{W}_{\text{DL}}$ ,  $\mathbf{b}_{\text{UL}}$ ,  $\mathbf{b}_{\text{DL}}$  are trainable parameters.

The predicted powers are then denormalized and rescaled to produce the final output  $\hat{\mathbf{p}} \in \mathbb{R}^{K \times 2}$ :

$$p_k^{\text{UL}} = \Delta_{\text{UL}} \tilde{p}_k^{\text{UL}} + \underline{P}_{\text{UL}}, \quad (19)$$

$$\hat{p}_k^{\text{DL}} = \frac{\tilde{p}_k^{\text{DL}} \sum_{l=1}^L \bar{P}_l^{\text{DL}}}{\sum_{k=1}^K \tilde{p}_k^{\text{DL}}}, \quad (20)$$

with

$$\check{p}_k^{\text{DL}} = \Delta_{\text{DL}} \tilde{p}_k^{\text{DL}} + \underline{P}_{\text{DL}}, \quad (21)$$

where  $\Delta_{\text{UL}} = \bar{P}_{\text{UL}} - \underline{P}_{\text{UL}}$  and  $\Delta_{\text{DL}} = \bar{P}_{\text{DL}} - \underline{P}_{\text{DL}}$  denote the UL and DL power ranges, respectively. Here,  $\bar{P}_{\text{UL}}$  and  $\underline{P}_{\text{UL}}$  are the maximum and minimum UL powers for UE  $k$ , while  $\bar{P}_{\text{DL}}$  and  $\underline{P}_{\text{DL}}$  are the corresponding DL bounds. The DL rescaling ensures that the total DL power budget across all APs is preserved.

## B. Attention mechanism

We now detail the attention mechanism used in (12). The queries ( $\mathbf{Q}$ ), keys ( $\mathbf{K}$ ), and values ( $\mathbf{V}$ ) [19] are simultaneously computed from the layer-normalized input  $\tilde{\mathbf{Z}}_{\text{in}}$  using a single linear transformation:

$$\mathbf{QKV} = \tilde{\mathbf{Z}}_{\text{in}} \mathbf{W}_{\text{qkv}} + \mathbf{b}_{\text{qkv}}, \quad (22)$$

where  $\mathbf{W}_{\text{qkv}} \in \mathbb{R}^{d_{\text{mod}} \times 3d_{\text{mod}}}$  and  $\mathbf{b}_{\text{qkv}} \in \mathbb{R}^{3d_{\text{mod}}}$  are trainable parameters. The resulting tensor  $\mathbf{QKV} \in \mathbb{R}^{B \times K \times 3d_{\text{mod}}}$  is split along the last dimension into three

parts, yielding  $\mathbf{Q}, \mathbf{K}, \mathbf{V} \in \mathbb{R}^{B \times K \times d_{\text{mod}}}$ . These are then reshaped into  $N_h$  attention heads of dimension  $d_{\text{head}} = d_{\text{mod}}/N_h$ , giving

$$\mathbf{Q}, \mathbf{K}, \mathbf{V} \in \mathbb{R}^{B \times N_h \times K \times d_{\text{head}}}. \quad (23)$$

A kernel feature mapping  $\phi(\cdot)$  is applied to the queries and keys:

$$\mathbf{Q}' = \phi(\mathbf{Q}), \quad (24)$$

$$\mathbf{K}' = \phi(\mathbf{K}), \quad (25)$$

with  $\phi(\cdot)$  being an activation function chosen to approximate the softmax kernel [31] of the original Transformer while enabling linearized attention.

The attention is then computed via a linearized operation:

$$\mathbf{A} = \mathbf{Q}' \cdot \left( (\mathbf{K}'^T \cdot \mathbf{V}) \cdot \mathbf{W} \right), \quad (26)$$

where  $\mathbf{W} \in \mathbb{R}^{K \times K}$  is a fixed cosine reweighting matrix with entries  $w_{ij} = \cos\left(\frac{\pi(i-j)}{2K}\right)$ . This modulation biases attention toward nearby tokens, mimicking the locality bias of softmax without computing full pairwise interactions, thereby avoiding the quadratic complexity. In our context, this allows the model to distinguish between nearby and distant UEs/APs without introducing additional trainable parameters.

Finally,  $\mathbf{A}$  is projected back into the model dimension, yielding the final attention weights used in (12):

$$\mathcal{A}(\tilde{\mathbf{Z}}_{\text{in}}) = \mathbf{A}\mathbf{W}_{\text{out}}^T + \mathbf{b}_{\text{out}}, \quad (27)$$

with  $\mathbf{W}_{\text{out}} \in \mathbb{R}^{d_{\text{mod}} \times d_{\text{mod}}}$  and  $\mathbf{b}_{\text{out}} \in \mathbb{R}^{d_{\text{mod}}}$  being trainable parameters.

Our choice of activation function. In the original CosFormer [24], the kernel feature mapping function  $\phi(\cdot)$  is implemented using ReLU. In this work, we propose a simple yet efficient modification: replacing ReLU with the ELU [31]. This choice is motivated by both physical insights and empirical evidence. Formally, the two activations are defined as [31]:

$$\begin{aligned} \text{ReLU}(x) &= \max(0, x), \\ \text{ELU}(x) &= \begin{cases} x & \text{if } x > 0, \\ \alpha(e^x - 1) & \text{if } x \leq 0, \end{cases} \end{aligned} \quad (28)$$

where  $\alpha$  is a hyperparameter, typically set to 1.

ELU provides smoother gradients and nonzero outputs for negative inputs, as illustrated in Fig. 4, thereby preserving richer feature interactions and improving gradient flow and numerical stability during training. This is particularly important in our setting, where spatial coordinates require the attention mechanism to capture subtle UE-AP variations. In contrast, ReLU zeroes out all negative inputs, potentially discarding useful spatial information and leading to sparse gradients that hinder convergence. By deliberately allowing negative values, ELU maintains continuity across the input domain and prevents inactive

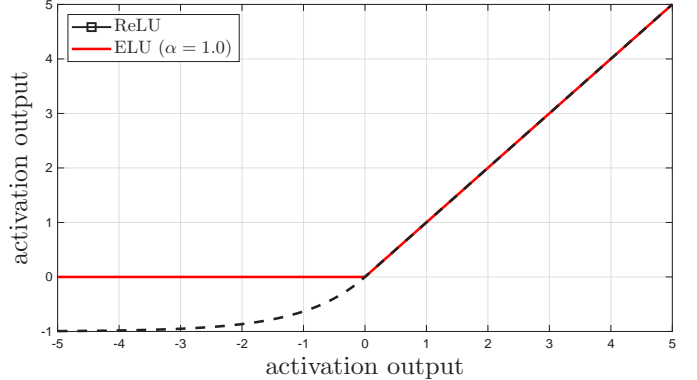


Fig. 4: Comparison of ReLU and ELU activation functions. ELU smoothly transitions for negative inputs using an exponential curve, improving gradient flow and stability.

attention heads, enabling the attention mechanism to exploit weak but meaningful AP-UE associations that would otherwise be suppressed. Such associations are critical under the max-min fairness criterion, where low-gain links can influence the performance of the worst-case user.

Moreover, the exponential tail of ELU produces a differentiable kernel that interacts harmoniously with the cosine modulation in (26), resulting in smoother and more stable attention distributions. This behavior aligns with the naturally smooth spatial variations in wireless propagation, leading to physically realistic clustering boundaries and balanced power allocation.

To validate this design choice, we evaluate the per-UE SE achieved by a CosFormer using several activations [31] with the simulation parameters in Table III. The results reported in Figs. 5 demonstrate that ELU consistently yields higher SE across all user counts  $K$  for both UL and DL scenarios, confirming that ELU provides a more effective kernel transformation for our problem.

## V. Training Setup

The model is trained offline to predict the AP clusters and UE powers. Next, we explain the structure of the generated dataset and provide details about the training process.

### A. Dataset construction

To train and evaluate the learning model, we construct a synthetic dataset that captures diverse cell-free network configurations and realistic deployment conditions. The dataset construction follows four main steps:

Step 1) Data generation: For each configuration defined by a pair  $(K, L)$ , we generate:

- random 2D positions within a bounded area for  $K$  single-antenna UEs, denoted as  $\{\mathbf{u}_k\}_{k=1}^K$ , with  $\mathbf{u}_k \in \mathbb{R}^2$ , and  $L$  uniformly distributed APs, denoted as  $\{\mathbf{a}_l\}_{l=1}^L$ , with  $\mathbf{a}_l \in \mathbb{R}^2$ ;
- Large-scale fading coefficients  $\beta_{lk}$  computed as in [11], which are required later by the

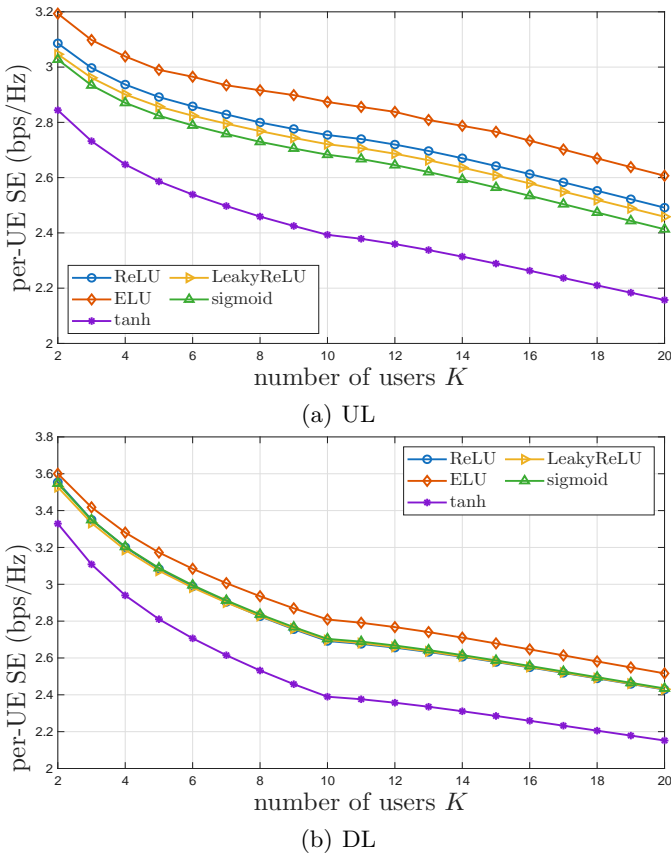


Fig. 5: Comparison of per-UE SE using different activation functions in CosFormer for UL and DL. ELU yields the highest SE across all UE counts.

closed-form solution to solve the max-min SE optimization problems in (9) and (10) for each set of clusters.

Step 2) Noise injection: To simulate localization errors and improve robustness, Gaussian noise is added to the UE and AP positions:

$$\mathbf{u}'_k = \mathbf{u}_k + \delta_k, \quad \delta_k \sim \mathcal{N}(0, \sigma_e^2), \quad (29)$$

$$\mathbf{a}'_l = \mathbf{a}_l + \delta_l, \quad \delta_l \sim \mathcal{N}(0, \sigma_e^2), \quad (30)$$

where  $\sigma_e = 1$  m, following [32]. This perturbation accounts for position estimation uncertainty in practice.

Step 3) Normalization: All features are normalized to the range  $[0, 1]$  using min-max scaling. For a feature vector  $\xi$ :

$$\tilde{\xi} = \frac{\xi - \min(\xi)}{\max(\xi) - \min(\xi) + \varepsilon}, \quad (31)$$

where  $\varepsilon$  is a small constant to avoid division by zero. Coordinates are normalized separately for  $x$  and  $y$ , preserving geometric relationships, while UL and DL powers are normalized globally to ensure consistent scaling.

---

#### Algorithm 1 Training with Dynamic Supervision

---

Require: Training dataset  $\{\mathbf{X}_i\}_{i=1}^S$ , batch size  $S$ , trade-off parameter  $\lambda$

- 1: for each epoch do
- 2:   for each batch do
- 3:     Compute attention scores from the input  $\mathbf{X}_i$
- 4:     Generate AP clusters for each UE
- 5:     Compute powers by solving (9) and (10) [11]
- 6:     Evaluate the loss function (32)
- 7:     Update model parameters via backpropagation
- 8: end for
- 9: end for

---

The normalized noisy positions are structured into an input  $\mathbf{X} \in \mathbb{R}^{K \times (2L+2)}$ , which feeds the model a sequence of  $K$  tokens. Each token represents one UE together with its relative information to all APs, aligning naturally with the token-based processing paradigm of Transformers. This design allows the attention mechanism to capture dependencies across users and identify which APs are most relevant for serving each UE, while ensuring generalization across different network sizes and topologies.

Step 4) Dataset overview: A total of 8000 training samples are generated for each value of  $K \in \{5, 10\}$  and  $L = 16$ . Each sample consists of normalized noisy UE and AP coordinates, with corresponding optimal powers computed on the fly during training. To evaluate generalization, additional samples are generated for other user counts beyond the training values of  $K$ , enabling assessment of the model's ability to adapt to unseen network configurations. Overall, the dataset includes diverse configurations by varying the number of UEs, their spatial distributions, and channel realizations, ensuring robust learning and effective generalization.

#### B. Training approach

Unlike standard supervised learning [33], the optimal powers cannot be precomputed before training because the clusters of APs serving each UE are determined dynamically by the model itself during each training epoch. The overall training procedure is summarized in Algorithm 1, which illustrates the dynamic supervision process where labels are generated on-the-fly based on intermediate model decisions.

During the forward pass of a training epoch, the model evaluates attention scores between the input features. These scores define the AP clusters, assigning to each UE a set of serving APs. Once the clusters are determined, the UL and DL power control problems are solved for the predicted clusters using the closed-form expression in [11]. The resulting optimal powers are then used in the

Table I: Model architecture parameters.

Parameter	Value
Encoder layers $M$	2
Attention heads $N_h$	4
Model dimension $d_{\text{mod}}$	64
Clustering threshold $\xi$	0.3

Table II: Model training hyperparameters.

Parameter	Value
Trade-off parameter $\lambda$	$10^{-2}$
Dropout rate	0.1
Optimizer	AdamW [37]
Learning rate	$10^{-3}$
Epochs	20
Batch size	64

backward pass to guide training. Specifically, the predicted powers  $\tilde{\mathbf{p}}$  are compared with the normalized optimal ones  $\mathbf{p}^*$ , and the loss function updates the model parameters:

$$\text{Loss} = \frac{1}{S} \sum_{i=1}^S \|\tilde{\mathbf{p}}_i^* - \tilde{\mathbf{p}}_i\|^2 - \lambda \left( \min_k \text{SE}_k^{\text{UL}} + \min_k \text{SE}_k^{\text{DL}} \right). \quad (32)$$

The loss combines the mean-squared error between predicted and optimal powers with a clustering-aware penalty term that promotes fairness across users. The hyperparameter  $\lambda$  controls the trade-off: larger values emphasize balancing the worst-case SE, while smaller values prioritize minimizing prediction error. In practice,  $\lambda$  is tuned empirically via cross-validation to achieve a balance between accuracy and fairness.

The model is implemented in PyTorch [34] and configured with the parameters listed in Tables I and II, empirically tuned to balance accuracy and computational efficiency.

Our training strategy follows a supervised learning paradigm with online label generation, also referred to as learning with dynamic supervision [35], [36]. In this framework, ground-truth labels are computed on-the-fly during training based on the model's intermediate decisions. Notably, the model does not take channel coefficients as input; instead, their effect is encapsulated in the optimal power labels. By learning directly from these labels, the network implicitly captures the propagation characteristics of the environment and learns to map UE-AP spatial configurations to clustering and power-allocation decisions. As a result, the model effectively approximates the max-min SE solution at inference time without requiring any explicit optimization.

## VI. Numerical results

In this section, we assess the performance of the proposed learning-based framework for solving the MMF problem in the user-centric cell-free mMIMO system described in Sect. II. The main simulation parameters are reported in Table III. All numerical results are averaged over the test set.

Table III: Cell-free mMIMO network parameters.

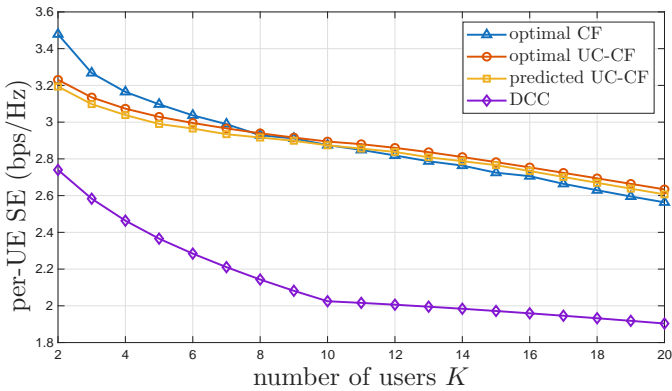
Parameter	Value
Network area	$500 \text{ m} \times 500 \text{ m}$
Number of APs ( $L$ )	16 (uniformly deployed)
Antennas per AP ( $N$ )	4
Carrier frequency	2 GHz
Path-loss exponent	3.67
UE-AP height difference	10 m
Shadow fading $F_{kl}$	$\mathcal{N}_{\mathbb{C}}(0, \alpha^2)$ , $\alpha^2 = 4 \text{ dB}$
Noise power $\sigma^2$	-94 dB
Noise figure $\eta$	7 dB
Bandwidth $B$	20 MHz
Max UL transmit power $\bar{P}_{\text{UL}}$	100 mW
Max DL transmit power per AP $\bar{P}_l^{\text{DL}}$	200 mW
Coherence block length $\tau_c$	200
Pilot length $\tau_p$	10
UL data symbols $\tau_u$	90
DL data symbols $\tau_d$	100

The proposed solution is compared against the following clustering and power-allocation schemes:

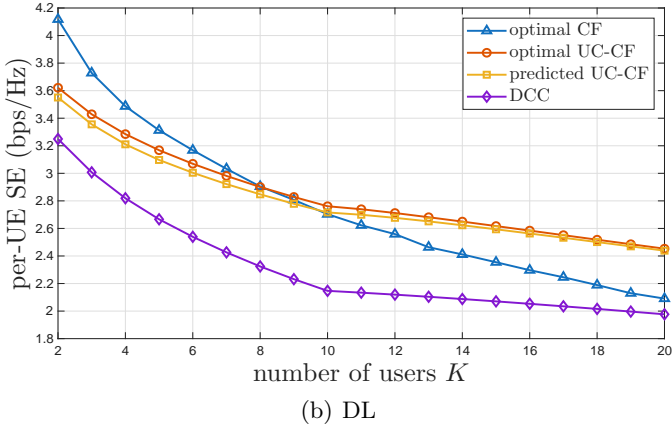
- Optimal CF: A fully cooperative baseline in which all APs serve all UEs, and transmit powers are obtained via the closed-form expression in [11].
- DCC: A fixed-clustering benchmark based on the dynamic cooperation clustering (DCC) scheme [9], where each UE is associated with its  $Q = 8$  strongest APs. Power control follows the closed-form solution.
- Optimal UC-CF: A hybrid strategy in which AP-UE clusters are inferred by the proposed model, while transmit powers are still computed using the closed-form solution.
- Predicted UC-CF: The fully data-driven approach, where both clustering decisions and power levels are directly predicted by the proposed learning architecture.

### A. Spectral efficiency evaluation

Fig. 6 reports the average per-UE SE as a function of the number of users  $K$  for both UL and DL transmission. As expected, the per-UE SE decreases with increasing  $K$  in both links, since a larger number of users must share a fixed amount of AP resources and is subject to higher interference. Nevertheless, the rate at which performance degrades varies significantly across the considered strategies. In the UL (Fig. 6a), Optimal CF provides the highest SE for small values of  $K$  due to full AP cooperation. However, its performance deteriorates more rapidly as  $K$  increases. Beyond  $K \approx 10$ , Optimal UC-CF surpasses the fully cooperative baseline, as limiting cooperation to the most relevant APs reduces interference and enables a more effective allocation of transmit power. A similar behavior is observed in the DL (Fig. 6b): while full cell-free (CF) remains superior at low user densities, Optimal UC-CF achieves higher SE for larger  $K$ , with the benefits of clustering being even more pronounced in DL due to improved power concentration and reduced inter-user interference. The Predicted UC-CF closely tracks the



(a) UL



(b) DL

Fig. 6: Average per-UE SE in UL and DL for different  $K$  values on the test set. The proposed model adapts better to increasing user load compared to benchmark policies.

optimal user-centric (UC)-CF in both UL and DL, confirming the generalization capability of the trained model across unseen user loads. In contrast, the classical DCC consistently yields the lowest SE, as its fixed clustering cannot adapt to varying interference conditions.

Overall, these results show that while fully cell-free operation is advantageous at low UE densities, user-centric clustering becomes increasingly beneficial as the network grows congested. The proposed learning model adapts to this transition, sustaining near-optimal performance with reduced computational and signaling overhead.

#### B. AP-UE clustering performance

In Fig. 7, we evaluate the total number of UE/AP connections (when UE is served by AP) of optimal CF, predicted UC-CF and DCC schemes for different user loads. In addition, we plot, in the secondary Y-axis, the average number of connections per UE of the predicted UC-CF.

The results show that the UC-CF scheme exhibits fewer total connections compared to CF, reflecting the selective association of users to a subset of APs based on the learned clustering. This indicates an efficient usage of network resources since less connections implies less signaling and

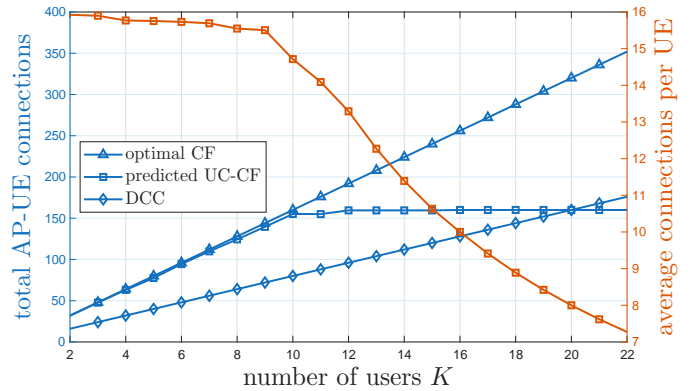


Fig. 7: Total AP-UE connections (left axis) and average connections per UE (right axis) as functions of different user loads. Our model in UC-CF strategy adapts the clusters dynamically to handle the increasing user load.

power consumption while still providing near-optimal SE as illustrated earlier in Fig. 6. Moreover, it can be seen that the total AP-UE connections saturates for higher user loads as the APs reach their  $\tau_p$ -served UE constraint unlike other policies that keep increasing, affecting their scalability. Correspondingly, the average number of APs per UE (red curve) gradually decreases as  $K$  increases. This behavior confirms the model's ability to dynamically reconfigure clusters and allocate AP efficiently under varying user densities to achieve better scalability. In contrast, the DCC, which always connects the UE to  $Q = 8$  APs, yields the low total connections at first, but at the expense of a poor SE performance (Fig. 6) and a linear growth of AP-UE connections with  $K$ .

Fig. 8 represents an example of the clustering behavior of the model for  $K = 20$  and  $L = 16$  for a given sample of the testing set. Each UE is annotated with the number of APs it is connected to, revealing the model's adaptive clustering. Dashed lines highlight the AP-UE links, showing selective association to only the most relevant APs. This visualization confirms that UC-CF forms compact, user-specific clusters that vary across users, enabling efficient resource allocation and reduced signaling overhead.

#### C. Power prediction accuracy

To further evaluate the effectiveness of the proposed learning model, we compare the cumulative distribution functions (CDFs) of UL and DL powers obtained from the optimal closed-form solution [11] and those predicted by the trained model on the test set. As shown in Fig. 9, the resulting curves are nearly overlapping in both cases, indicating that the model successfully learns the underlying power allocation strategy for the predicted clusters. This close agreement demonstrates that the predicted powers not only approximate the optimal allocation with high fidelity but also preserve the statistical distribution of transmit powers across UEs. Consequently, the proposed

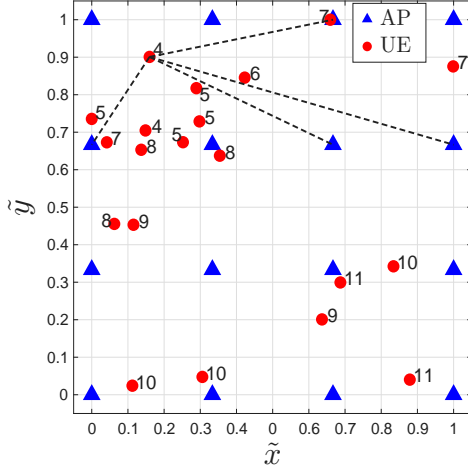
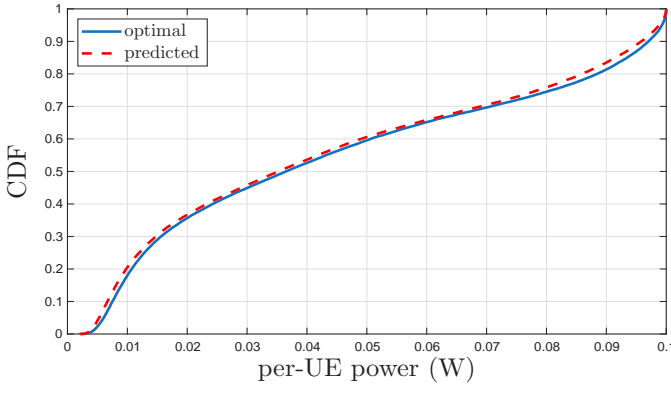
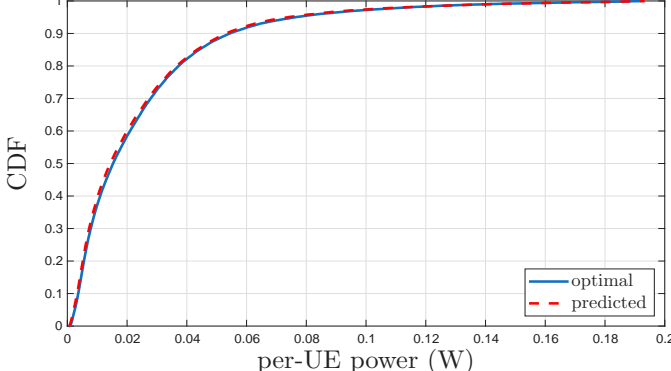


Fig. 8: Network layout of APs and UEs for  $K = 20$  users. User-specific clusters are predicted by the model for efficient resource allocation.



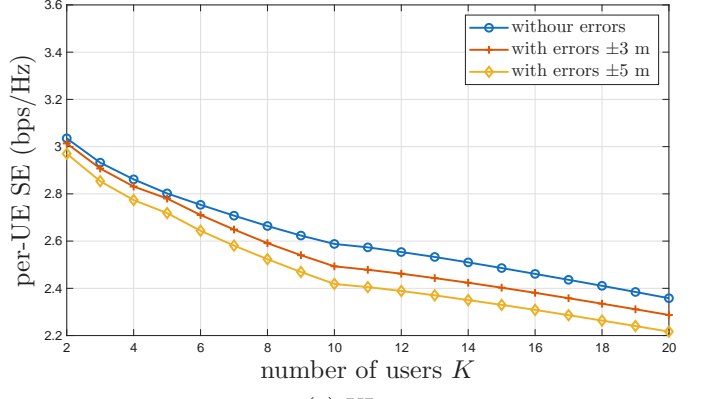
(a) CDF of UL transmit powers.



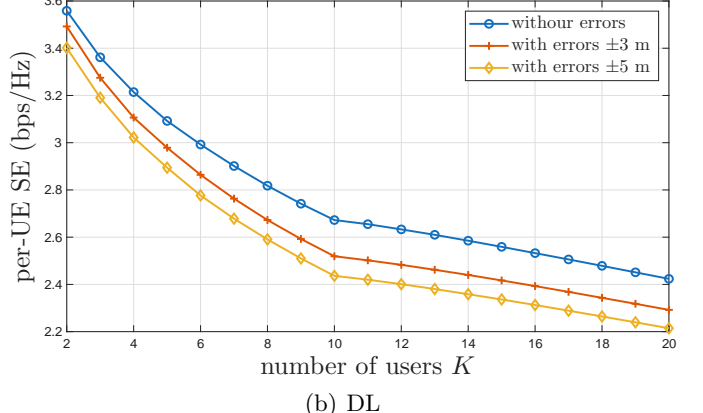
(b) CDF of DL transmit powers.

Fig. 9: CDF comparison of optimal and predicted powers in UL and DL. The close overlap confirms the accuracy of the proposed learning model in reproducing the optimal power statistics.

approach achieves reliable power prediction while avoiding the computational burden of solving the closed-form optimization problem.



(a) UL



(b) DL

Fig. 10: Average per-UE SE for different UE counts and input error levels. The trained model remains robust to input errors.

#### D. Robustness to input errors

In Fig. 10, we analyze the robustness of the proposed learning model against input uncertainty. During training, the model is exposed to user position inputs corrupted by random Gaussian noise with a standard deviation of 1 m. To assess generalization and robustness, the model is evaluated under three test conditions: i) input with a fixed standard deviation error of 3 m, ii) input with a fixed standard deviation error of 5 m, and iii) an ideal scenario with error-free input.

The results show that the per-UE SE decreases only slightly as the input error level increases, for both UL and DL. Specifically, the maximum gap between the error-free and 5 m error cases is approximately 0.29 b/s/Hz in UL and 0.24 b/s/Hz in DL across all user counts, demonstrating the resilience of the proposed model. Moreover, the relative trends across different user loads are preserved, indicating that the model can generalize its learned spatial relationships even when the inputs are affected by localization errors, thus ensuring practical robustness for real-world deployments where user position estimates are inherently imperfect.

Table IV: Performance comparison of Transformer variants in terms of complexity and efficiency metrics.

Model	Parameters	Memory (MB)	FLOPs	Latency (ms)	Training Time (s/epoch)
ELU-CosFormer	103,378	0.39	1,056,820	3.42	858.27
CosFormer	103,378	0.39	1,056,820	3.40	915.82
Transformer	846,866	3.23	5,682,260	4.42	1447.69
Longformer	7,102,738	27.09	635,398,900	680.99	1866.63
Performer	103,378	0.39	1,041,460	4.40	1076.56

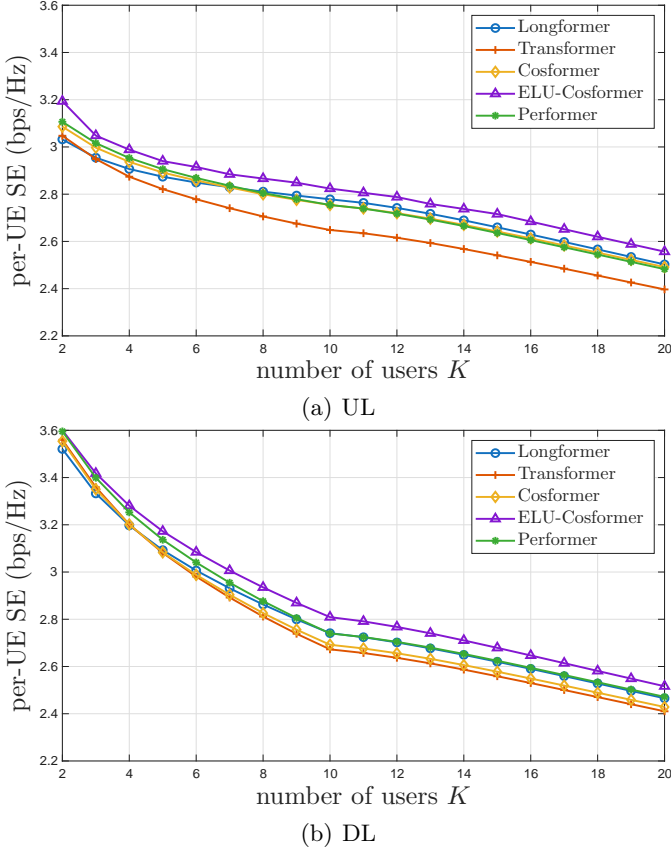


Fig. 11: Comparison of per-UE SE across different Transformer variants for UL and DL scenarios. Our modified CosFormer maintains higher SE.

### E. Comparison with other Transformer variants

Fig. 11 presents a comparative analysis of UL and DL per-UE SE achieved by the Transformer and four linear attention variants. Linformer is excluded because it cannot accommodate variable UE counts without additional preprocessing or architectural modifications [26].

In both UL and DL scenarios, ELU-CosFormer consistently outperforms the other models across all user counts. This confirms the effectiveness of integrating the ELU activation into the CosFormer kernel. CosFormer also shows strong performance, closely trailing ELU-CosFormer, while Performer and Transformer achieve moderate SE levels. Longformer, although competitive at low user counts, exhibits a steeper decline as  $K$  increases, indicating reduced scalability. The superior per-

formance of ELU-CosFormer stems from the integration of ELU with CosFormer's cosine-based attention kernel, as explained in Section IV. As a result, ELU-CosFormer forms physically consistent clusters and outperforms other variants across all user counts under our fairness-driven objective.

In addition to SE, Table IV compares the models in terms of complexity and efficiency metrics. All models were evaluated under consistent conditions to ensure fair comparison, with latency and training time reported for  $K = 10$  UEs.

- Parameters: Total number of trainable weights in the model.
- Memory (MB): Estimated memory footprint during inference, reflecting GPU usage.
- FLOPs: Floating-point operations per forward pass, indicating computational complexity.
- Latency (ms): Average inference time, measuring real-time responsiveness.
- Training Time (s/epoch): Time per training epoch, capturing training efficiency.

ELU-CosFormer and CosFormer share the same architecture and parameter count, differing only in their activation functions-ELU and ReLU, respectively. Although ELU is computationally more intensive, ELU-CosFormer achieves slightly lower training time per epoch, likely due to smoother gradient flow that enables more efficient back-propagation and faster convergence. In contrast, ReLU's simplicity gives CosFormer a marginal advantage in inference latency, as ReLU operations are highly optimized for GPU execution. Performer maintains a low parameter count and memory footprint comparable to CosFormer, but exhibits higher training and inference times due to the computational overhead of random feature projections and exponentiation in its kernel mapping [25], which are less GPU-efficient than CosFormer's cosine reweighting.

The standard Transformer exhibits substantially higher FLOPs and memory requirements, owing to its quadratic attention mechanism and larger parameter count, resulting in increased latency and longer training time. Longformer shows the highest latency and training time overall, reflecting its significantly larger parameter count relative to the other models.

In summary, the results in Fig. 11 and Table IV indicate that the proposed ELU-CosFormer achieves the most balanced and scalable performance, validating its design for fairness-aware resource optimization.

## VII. Computational Complexity Analysis

When the number of users  $K$  increases, the per-sample computational complexity of our model is dominated by the linearized attention term  $\mathcal{O}(M \cdot d_{\text{mod}} \cdot K)$ , which scales linearly with  $K$ . This linear scaling represents a clear advantage compared to prior Transformer-based approaches [20], [23], where the complexity grows quadratically as  $\mathcal{O}(M \cdot d_{\text{mod}} \cdot K^2)$ , and iterative optimization methods [10], which scale as  $\mathcal{O}(T \cdot L \cdot K^2)$  with  $T$  iterations. It is also favorable compared to the optimal closed-form solution that require cubic scaling  $\mathcal{O}(K^3)$ , which quickly become prohibitive in dense networks.

For illustration, we benchmark the runtime on a CPU for  $K = 40$ , computing both AP-UE clusters and UL/DL powers using our predicted UC-CF scheme versus DCC (with closed-form solution for power computation). The proposed UC-CF model requires only 9.2 ms, whereas DCC takes 31.6 s. This orders-of-magnitude speedup, achieved through linearized attention, highlights the significant efficiency gain of our approach and makes it more suitable for large-scale deployments.

Beyond asymptotic complexity, several practical aspects reinforce the advantage of our model. The linear attention mechanism reduces memory usage compared to quadratic approaches, enabling scalability to larger user counts and deployment on resource-constrained edge devices. This efficiency also translates into lower energy consumption, aligning with sustainability goals in next-generation wireless networks. Moreover, the one-shot inference design avoids iterative overhead, ensuring real-time responsiveness to dynamic user distributions and mobility. Importantly, the model maintains near-optimal SE despite its reduced complexity, confirming that efficiency does not compromise accuracy. Finally, linear attention benefits more from parallelization on graphics processing unit and tensor processing unit [38], [39], further widening the performance gap with quadratic and iterative methods.

## VIII. Conclusion

This paper proposed a scalable and flexible deep learning model for joint AP clustering and power allocation in user-centric cell-free massive MIMO systems. By relying only on spatial information and leveraging a customized CosFormer attention mechanism, our approach eliminates the need for channel estimation, avoids pilot contamination, and adapts seamlessly to dynamic network configurations. Numerical evaluations demonstrate that the proposed method achieves near-optimal SE with significantly reduced computation and signaling overhead, making it a practical solution for dynamic and large-scale systems.

Future research directions include investigating distributed learning strategies among APs or clusters to further reduce centralization requirements. Another promising direction is the integration of temporal information, enabling the model to capture user mobility, traffic variations, and time-dependent channel dynamics. Extending

the architecture with temporal attention mechanisms may enable proactive resource allocation and enhance robustness in highly dynamic operating conditions.

## References

- [1] H. Q. Ngo, A. Ashikhmin, H. Yang, E. G. Larsson, and T. L. Marzetta, "Cell-free massive MIMO versus small cells," vol. 16, no. 3, pp. 1834–1850, 2017.
- [2] ———, "Cell-free massive MIMO: Uniformly great service for everyone," in Proc. IEEE Intl. Work. Signal Process. Advances in Wireless Commun. (SPAWC). Stockholm, Sweden: IEEE, 2015, pp. 201–205.
- [3] E. Nayebi, A. Ashikhmin, T. L. Marzetta, and H. Yang, "Cell-free massive MIMO systems," in Proc. Asilomar Conf. Signals, systems, and computers. Pacific Grove, CA, USA: IEEE, 2015, pp. 695–699.
- [4] E. Björnson and L. Sanguinetti, "Making cell-free massive MIMO competitive with MMSE processing and centralized implementation," vol. 19, no. 1, pp. 77–90, 2019.
- [5] H. Q. Ngo, G. Interdonato, E. G. Larsson, G. Caire, and J. G. Andrews, "Ultradense cell-free massive MIMO for 6G: technical overview and open questions," vol. 112, no. 7, pp. 805–831, 2024.
- [6] Ö. T. Demir, E. Björnson, and L. Sanguinetti, "Foundations of user-centric cell-free massive MIMO," Foundations and Trends® in Signal Processing, vol. 14, no. 3-4, pp. 162–472, 2021.
- [7] S. Buzzi and C. D'Andrea, "Cell-free massive MIMO: User-centric approach," vol. 6, no. 6, pp. 706–709, 2017.
- [8] S. Buzzi, F. Linsalata, E. Moro, and G. Interdonato, "Why user-centric cell-free distributed MIMO systems will be the disruptive 6G technology," Authorea Preprints, 2025.
- [9] E. Björnson and L. Sanguinetti, "A new look at cell-free massive MIMO: Making it practical with dynamic cooperation," in Proc. IEEE Intl. Symp. Personal, Indoor and Mobile Radio Communications (PIMRC). Istanbul, Turkey: IEEE, 2019, pp. 1–6.
- [10] M. Farooq, H. Q. Ngo, and L.-N. Tran, "Accelerated projected gradient method for the optimization of cell-free massive MIMO downlink," in Proc. IEEE Intl. Symp. Personal, Indoor and Mobile Radio Commun. (PIMRC), London, UK, 2020.
- [11] L. Miretti, R. L. G. Cavalcante, S. Stańczak, M. Schubert, R. Böhnke, and W. Xu, "Closed-form max-min power control for some cellular and cell-free massive MIMO networks," in Proc. IEEE Veh. Technol. Conf. (VTC), Helsinki, Finland, 2022.
- [12] E. Shi, J. Zhang, J. An, G. Zhang, Z. Liu, C. Yuen, and B. Ai, "Joint AP-UE association and precoding for SIM-aided cell-free massive MIMO systems," vol. 24, no. 6, pp. 5352–5367, 2025.
- [13] E. Björnson, E. Jorswieck et al., "Optimal resource allocation in coordinated multi-cell systems," Foundations and Trends® in Communications and Information Theory, vol. 9, no. 2-3, pp. 113–381, 2013.
- [14] H. A. Ammar, R. Adve, S. Shahbazpanahi, G. Boudreau, and K. V. Srinivas, "User-centric cell-free massive MIMO networks: A survey of opportunities, challenges and solutions," vol. 24, no. 1, pp. 611–652, 2021.
- [15] G. Di Gennaro, A. Buonanno, G. Romano, S. Buzzi, and F. A. Palmieri, "A deep learning approach for user-centric clustering in cell-free massive MIMO systems," in Proc. IEEE Intl. Work. Signal Process. Advances in Wireless Commun. (SPAWC), Lucca, Italy, 2024, pp. 661–665.
- [16] A. Liu and V. K. Lau, "Joint BS-user association, power allocation, and user-side interference cancellation in cell-free heterogeneous networks," vol. 65, no. 2, pp. 335–345, 2016.
- [17] H. A. Ammar, R. Adve, S. Shahbazpanahi, G. Boudreau, and K. V. Srinivas, "Downlink resource allocation in multiuser cell-free MIMO networks with user-centric clustering," vol. 21, no. 3, pp. 1482–1497, 2021.
- [18] Z. Liu, J. Zhang, Z. Liu, D. W. K. Ng, and B. Ai, "Joint cooperative clustering and power control for energy-efficient cell-free XL-MIMO with multi-agent reinforcement learning," vol. 72, no. 12, pp. 7772–7786, 2024.

- [19] A. Vaswani, N. Shazeer, N. Parmar, J. Uszkoreit, L. Jones, A. N. Gomez, L. Kaiser, and I. Polosukhin, "Attention is all you need," in Proc. Conf. Neural Inf. Process. Systems (NIPS), Long Beach, CA, USA, 2017.
- [20] A. K. Kocharlakota, S. A. Vorobyov, and R. W. Heath Jr, "Pilot contamination aware transformer for downlink power control in cell-free massive MIMO networks," arXiv preprint arXiv:2411.19020, 2024.
- [21] M. Dwarampudi and N. Reddy, "Effects of padding on LSTMs and CNNs," arXiv preprint arXiv:1903.07288, 2019.
- [22] F. Alrasheedi, X. Zhong, and P.-C. Huang, "Padding module: Learning the padding in deep neural networks," vol. 11, pp. 7348–7357, 2023.
- [23] I. Chafaa, G. Bacci, and L. Sanguinetti, "Transformer-based power optimization for max-min fairness in cell-free massive MIMO," vol. 14, no. 8, pp. 2316–2320, 2025.
- [24] Z. Qin, W. Sun, H. Deng, D. Li, Y. Wei, B. Lv, J. Yan, L. Kong, and Y. Zhong, "cosFormer: Rethinking softmax in attention," arXiv preprint arXiv:2202.08791, 2022.
- [25] K. Choromanski, V. Likhoshesterov, D. Dohan, X. Song, A. Gane, T. Sarlos, P. Hawkins, J. Davis, A. Mohiuddin, L. Kaiser, D. Belanger, L. Colwell, and A. Weller, "Rethinking attention with performers," arXiv preprint arXiv:2009.14794, 2020.
- [26] S. Wang, B. Z. Li, M. Khabsa, H. Fang, and H. Ma, "LinFormer: Self-attention with linear complexity," arXiv preprint arXiv:2006.04768, 2020.
- [27] I. Beltagy, M. E. Peters, and A. Cohan, "Longformer: The long-document transformer," arXiv preprint arXiv:2004.05150, 2020.
- [28] S. Chakraborty, E. Björnson, and L. Sanguinetti, "Centralized and distributed power allocation for max-min fairness in cell-free massive MIMO," in Proc. Asilomar Conf. Signals, systems, and computers. Pacific Grove, CA, USA: IEEE, 2019, pp. 576–580.
- [29] D. Kim, H. Jung, and I.-H. Lee, "A survey on deep learning-based resource allocation schemes," in Proc. Intl. Conf. Information and Commun. Technol. Convergence (ICTC), Jeju Island, South Korea, 2023.
- [30] Q. Mao, F. Hu, and Q. Hao, "Deep learning for intelligent wireless networks: A comprehensive survey," vol. 20, no. 4, pp. 2595–2621, 2018.
- [31] A. D. Rasamoelina, F. Adjailia, and P. Sinčák, "A review of activation function for artificial neural network," in Proc. IEEE World Symp. Applied Machine Intell. & Informatics (SAMI), Herlany, Slovakia, 2020.
- [32] C. Xue, P. Psimoulis, Q. Zhang, and X. Meng, "Analysis of the performance of closely spaced low-cost multi-gnss receivers," Applied Geomatics, vol. 13, no. 3, pp. 415–435, 2021.
- [33] V. Nasteski, "An overview of the supervised machine learning methods," Horizons. b, vol. 4, no. 51-62, p. 56, 2017.
- [34] A. P. et al., "PyTorch: An imperative style, high-performance deep learning library," in Proc. Conf. Neural Inf. Process. Systems (NIPS), Vancouver, Canada, 2019.
- [35] H. Pham, Z. Dai, Q. Xie, and Q. V. Le, "Meta pseudo labels," in Proceedings of the IEEE/CVF conference on computer vision and pattern recognition, 2021, pp. 11557–11568.
- [36] X. Wang, Z. Xu, D. Yang, L. Tam, H. Roth, and D. Xu, "Learning image labels on-the-fly for training robust classification models," arXiv preprint arXiv:2009.10325, 2020.
- [37] P. Zhou, X. Xie, Z. Lin, and S. Yan, "Towards understanding convergence and generalization of AdamW," vol. 46d, no. 9, pp. 6486–6493, 2024.
- [38] S. Pal, V. Zhang, E. Ebrahimi, S. Migacz, A. Zulfiqar, Y. Fu, D. Nellans, and P. Gupta, "Optimizing multi-GPU parallelization strategies for deep learning training," arXiv preprint arXiv:1907.13257, 2019.
- [39] N. P. Jouppi, C. Young, N. Patil, D. Patterson, G. Agrawal, R. Bajwa, S. Bates, S. Bhatia, N. Boden, A. Borchers et al., "In-datacenter performance analysis of a tensor processing unit," in Proc. Annual Intl. Symp. Computer Architecture, Toronto, Canada, 2017, pp. 1–12.